Available on CMS information server

CMS CR -2017/431

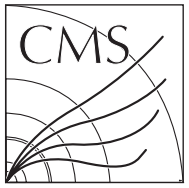

The Compact Muon Solenoid Experiment

Conference Report

Mailing address: CMS CERN, CH-1211 GENEVA 23, Switzerland

23 November 2017 (v2, 06 December 2017)

Large-Area Silicon Detectors for the CMS High Granularity Calorimeter

Elias Pree for the CMS Collaboration

Abstract

During the so-called Phase-2 Upgrade, the CMS experiment at CERN will undergo significant improvements to cope with the 10-fold luminosity increase of the High Luminosity LHC (HL-LHC) era. Especially the forward calorimetry will suffer from very high radiation levels and intensified pileup in the detectors. For this reason, the CMS collaboration is designing a High Granularity Calorimeter (HGCAL) to replace the existing endcap calorimeters. It features unprecedented transverse and longitudinal segmentation for both electromagnetic (CE-E) and hadronic (CE-H) compartments. The CE-E and a large fraction of CE-H will consist of a sandwich structure with silicon as active detector material. This paper presents an overview of the ongoing sensor development for the HGCAL and highlights important design features and measurement techniques. The design and layout of an 8-inch silicon sensor prototype is shown. The hexagonal sensors consist of 235 pads, each with an area of about 1 cm^2. Furthermore, Synopsys TCAD simulations regarding the high voltage stability of the sensors for different geometric parameters are performed. Finally, two different IV characterisation methods are compared on the same sensor.

Presented at *CHEF2017 Calorimetry for the High Energy Frontier 2017*

Prepared for submission to JINST

2nd CHEF Conference
2-6 October 2017
Lyon, France

Large-Area Hexagonal Silicon Detectors for the CMS High Granularity Calorimeter

E. Pree,[a,1] **on behalf of the CMS collaboration**

[a] *Institute of High Energy Physics, Austrian Academy of Sciences, Vienna, Austria*

E-mail: elias.pree@oeaw.ac.at

Abstract: During the so-called Phase-2 Upgrade, the CMS experiment at CERN will undergo significant improvements to cope with the 10-fold luminosity increase of the High Luminosity LHC (HL-LHC) era. Especially the forward calorimetry will suffer from very high radiation levels and intensified pileup in the detectors. For this reason, the CMS collaboration is designing a High Granularity Calorimeter (HGCAL) to replace the existing endcap calorimeters. It features unprecedented transverse and longitudinal segmentation for both electromagnetic (CE-E) and hadronic (CE-H) compartments. The CE-E and a large fraction of CE-H will consist of a sandwich structure with silicon as active detector material. This paper presents an overview of the ongoing sensor development for the HGCAL and highlights important design features and measurement techniques. The design and layout of an 8-inch silicon sensor prototype is shown. The hexagonal sensors consist of 235 pads, each with an area of about 1 cm^2. Furthermore, Synopsys TCAD simulations regarding the high voltage stability of the sensors for different geometric parameters are performed. Finally, two different IV characterisation methods are compared on the same sensor.

Keywords: Materials for solid-state detectors; Manufacturing; Si microstrip and pad detectors

[1] Corresponding author.

Contents

1 The High Granularity Calorimeter at the CMS Experiment **1**

2 Design and Layout of HGC Sensors **2**

3 TCAD Simulation **3**

4 Sensor Measurements **4**

5 Summary **6**

1 The High Granularity Calorimeter at the CMS Experiment

The Large Hadron Collider (LHC) at CERN will undergo a major luminosity upgrade [1] after the Long Shutdown 3 (LS3) around 2026. An increase of the instantaneous luminosity by a factor 5 to 7 in comparison to the current state is planned. The integrated luminosity after 10 years of operation is expected to be 3000 fb^{-1}. Numerous systems in the CMS experiment [2] cannot cope with the increased number of collisions or have to be replaced because they reached the end of their designated lifetime due to radiation damage. The upgrades during this period are referred to as CMS Phase-2 upgrade. One system that needs to be upgraded is the Endcap Calorimeters.
In the current implementation of the CMS Calorimeter Endcap, a $PbWO_4$-based electromagnetic and a plastic scintillator based hadronic calorimeter can be found. They were designed for an integrated luminosity of 500 fb^{-1} and therefore have to be replaced due to too large performance degradation after LS3.

The new High Granularity Calorimeter (HGCAL) features unprecedented transverse and longitudinal segmentation. This will facilitate particle-flow calorimetry, where the fine structure of showers can be determined and used to enhance pile-up rejection and particle identification whilst still achieving good energy resolution. The new calorimeter consists of an electromagnetic part called CE-E, which contains 28 sampling layers. Here, silicon sensors are used as active material and steel-clad lead as main absorber. On Figure 1b, a more detailed view of the cross section of a double-sided layer is shown. Next to the electromagnetic part, the calorimeter also consists of a hadronic part called CE-H. It has 8 silicon sampling layers and 16 layers where both silicon sensors and silicon photomultipliers mounted directly on tiles of plastic scintillators, are used. The silicon sensor part is shown in green and the scintillator part in blue in Figure 1a. About 600 m^2 of silicon, or 27000 8-inch silicon wafers, are needed in total. Initially proposed 6-inch wafers for the HGCAL project are described in works like [3]. The decision to go from 6-inch to 8-inch was driven by arguments like reduced costs and less complexity, because less sensor modules are required. Since the viability of 8-inch silicon sensors was previously also investigated, for example for the CMS Tracker in [4], 8-inch sensors became the new standard for the HGCAL project.

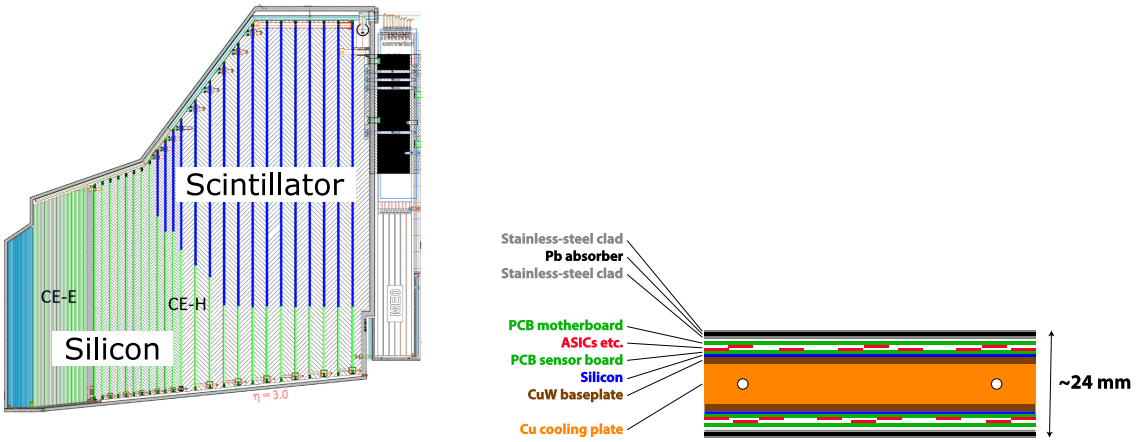

(a) (b)

Figure 1: Sketch of the new High Granularity Calorimeter Endcap (a). The part with silicon as active material is highlighted in green, the scintillator region in blue. The cross section of the arrangement of the different layers showing silicon as active material and absorbers is shown in the second plot (b). Two silicon modules are mounted on each side of a Cu cooling plate and surrounded by steel-clad lead absorber plates.

2 Design and Layout of HGC Sensors

Sensors in the endcap with lower radial distance to the interaction point receive a higher fluence in comparison to sensors with higher radial distance. With increased neutron fluence the signal yield of a silicon sensor decreases [5, 7]. Using thinner sensors increases the signal in electrons/µm for the same fluence. Hence, three regions with different sensor thicknesses were defined to account for the different fluence regions. In the highest fluence region, fluences up to 1.0×10^{16} $n_{eq}cm^{-2}$ are expected. Because of this the smallest wafer thickness of 120 µm is chosen here. For the second region, for fluences up to 2.5×10^{15} n_{eq} cm^{-2}, sensors will have a thickness of 200 µm. The third region contains 300 µm thick sensors for fluences up to 5.0×10^{14} n_{eq} cm^{-2}.

Due to radiation damage, the full depletion voltage of a p-type silicon sensor will increase. This statement also holds for n-type sensors after type inversion. Therefore, the sensors need to be operated at higher voltage in comparison to unirradiated sensors. For this project, the sensors are planned to be operated at 800 V after 3000 fb^{-1} but should be designed to withstand 1 kV. This introduces some considerations to the sensor design, which will be adressed by simulations in Section 3.

A hexagonal sensor geometry was chosen, because it is a tile-able polygon with the highest possible number of corners. Using the space on a circular wafer most efficiently is an important aspect to reduce costs. A hexagonal sensor contains many individual cells, which are mostly smaller hexagons with an area of either 0.5 cm^2 or about 1.0 cm^2. Each individual cell is a diode, which is implemented by a thin implant of opposed bulk polarity with the desired pad area, and a metal layer on top of each cell. For the 120 µm and 200 µm thick sensors, these diodes will be p-type. For the 300 µm thick sensors, the type is not yet decided. Although the performance of p-type under

irradiation [6] is better than n-type, its cost is higher. N-Type sensors require a smaller number of photolithography masks in sensor production than p-type sensors.
The layout of an 8-inch prototype sensor for HGCAL is shown in Figure 2. It contains 235 cells. Most are hexagonal, but some - at the edges and corners of the sensor - have truncated tips to facilitate assembly of the sensors into modules. The spacing between cells varies between 20 µm and 80 µm, in order to study noise and breakdown. Two of the hexagonal cells are divided into an inner small hexagon and a surrounding area. The former is to facilitate calibration with minimum-ionizing particles. The sensor cells are surrounded by two guard rings and one edge ring. The inner guard ring is on the same potential as the cells, while the outer guard ring is floating. The inner guard ring is not floating to avoid the coupling of one signal of a cell to a neighbouring cell via this guard ring. As there is no common biasing grid for all cells of the whole sensor, each pad has to be biased individually.

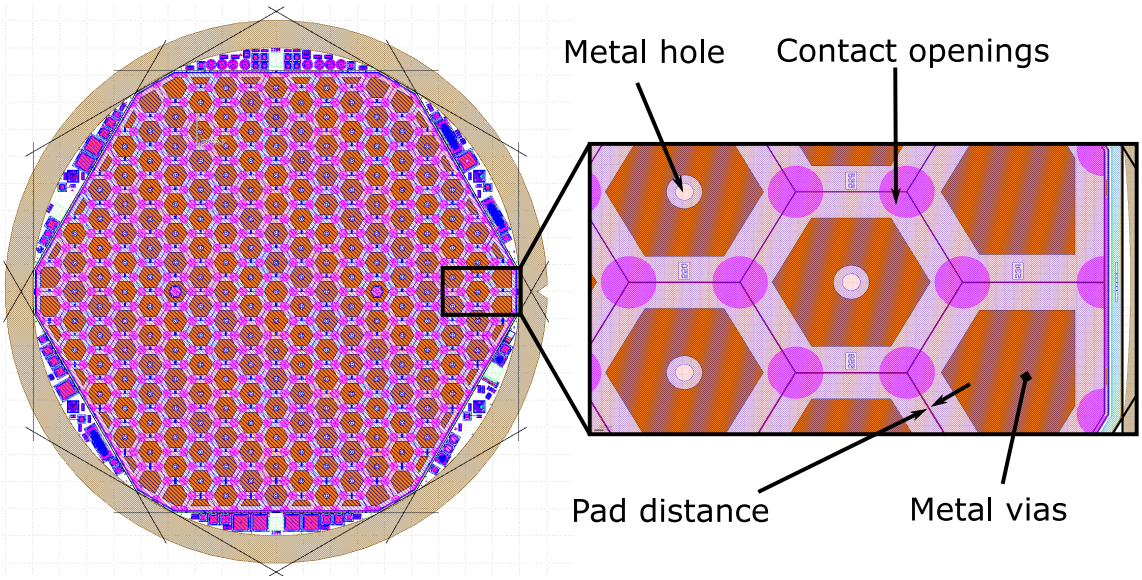

Figure 2: Screenshot of the design of an 8 inch prototype sensor for HGCAL. The figure on the right shows an enlarged version of a sensor cell. Important design features like metal holes for laser irradiation or contact openings are indicated with black arrows.

3 TCAD Simulation

In order to optimize future designs we started simulations with Synopsys TCAD [8], which is based on the finite element method. Hence, the geometry is discretised with a mesh, and equations (e.g. Poisson equation) are solved on the mesh nodes. This method works for 2D and 3D problems. For the simulations presented here, the problem was reduced to two dimensions.
Figure 3 show the simulation results of a breakdown simulation of the inter-cell (= pad) area of two pads on a p-type sensor. Both pads are on ground potential, and high voltage is applied on the back side. A 6 µm wide p-stop implant is implemented between the pads to improve the electrical separation of the individual diodes. Figure 3b shows the geometry, while also showing the electric

field at -2250 V, 109 V above breakdown. Two important parameters that were varied are the pad distance and the metal overhang of the cell. The pad distance is the distance between the edge of the implant of one cell to the edge of the implant of the neighbour cell. The metal overhang is the width of the protruding metal layer on top of the n-type implant of the pad.

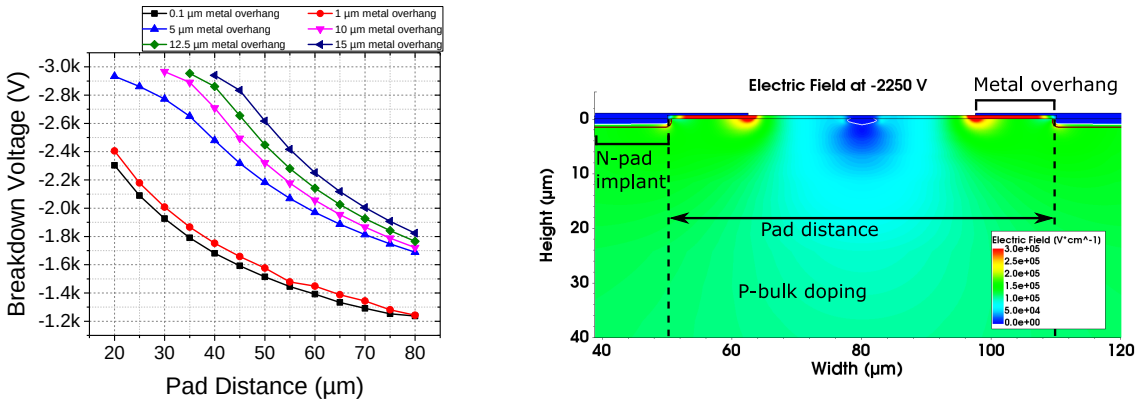

(a) (b)

Figure 3: Results of a breakdown simulation with varying metal overhang and pad distance, where both pads on top are on the same potential. Increasing pad distance leads to smaller breakdown voltages, while increasing the metal overhang leads to higher breakdown voltages (a). The electric field at -2250 V for 60 µm pad distance with 12.5 µm metal overhang is shown (b).

According to Figure 3a, the breakdown voltage decreases when the pad distance increases from 20 µm to 80 µm. On the other hand, the breakdown voltage increases when the metal overhang increases from 0.1 µm to 15 µm. One can also see that the improvement in breakdown voltage is largest between 1 µm and 5 µm metal overhang. Therefore, this simulation suggests that the metal overhang should always be larger than 5 µm. For pad distances larger than 40 µm, the metal overhang can be up to 15 µm to optimize the breakdown voltage. In comparison, the design introduced in Section 2 features a metal overhang of 5 µm and 12.5 µm. The former value is used for sensor cells with a pad distance of 20 µm and the later for all others. It should be mentioned that the quantitative voltage value of the breakdown simulation in Figure 3a is not meaningful. The qualitative trend, when changing simulation parameters, is of importance.
When investigating Figure 3b, the red areas are of most interest. They indicate areas where the electric field in the bulk is at least 300 kV/cm and the avalanche condition is met. This means the sensor breakdown will occur there. In this simulation, the highest field was always at the outer edge of the metal overhang. If the metal overhang is too small, this high field region will coincide with the electric field peak near the edge of the pad implant and lead to early breakdown. This behaviour can be seen in Figure 3a as the black and red lines.

4 Sensor Measurements

Measurements were performed on the prototype sensors with a thickness of 200 µm. Figure 4 shows current measurements at -100 V for one sensor with the geometry introduced in Section 2.

The sensors have a full depletion voltage of about 60 V. In Figure 4a, a current measurement with a single needle is shown. Only one cell is contacted and set to ground potential, while all other cells are floating. At the same time, high potential, ranging from 0 V up to 1 kV, is applied to the back side of the sensor. With this measurement method, the different quadrants with different pad distances can be distinguished by the different currents measured. With decreasing pad distance, increasing current is measured. This is the opposite behaviour in comparison to Section 3, where decreasing pad distance suggests higher breakdown voltage. This would commend the same or smaller current. In the simulation, the pad and its neighbour are on the same potential, but here the neighbouring pads are floating. This means that the full depletion region can spread out laterally, and hence the current measured is increased by the neighbours. Larger pad distances mean larger inter-pad resistance and the spread of the depletion region and the current measured on the pads is reduced. Additionally, defective cells that feature an earlier breakdown and higher current influence the surrounding pads as well. An increase in current can then be seen in the surrounding cells as well.

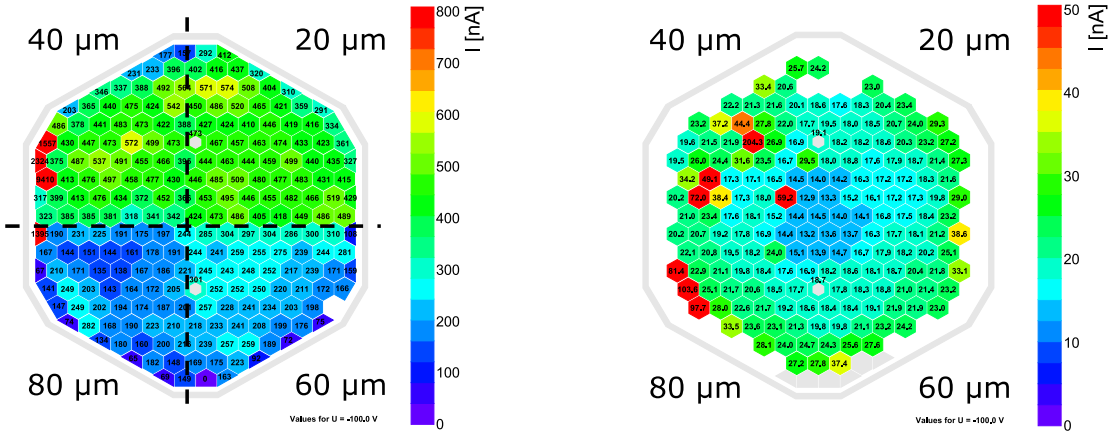

(a) (b)

Figure 4: Single-needle measurement of an 8-inch prototype sensor is shown (a). Quadrants with different pad distances result in different measured currents. Seven-needle measurement on the same 8-inch prototype sensor (b) do not show this dependence at -100 V. The observed radial change in current is related to lithography problems during sensor processing.

On Figure 4b, an alternative measurement method with seven needles instead of a single one is used on the same sensor. In this configuration, the six neighbour cells are put to the same potential as the cell under investigation. Hence, the depletion region is confined to this pad only, and the measured currents are much smaller. The median with standard deviation of the current of all pads with the single needle measurement method (4a) is $(3.1\times10^{-7}\pm1.3\times10^{-7})$ A. The defect cells were excluded from the median and standard deviation calculation. A cell is counted as a defect cell, if the current exceeds 1000 nA. For the seven needle configuration (4b) the median with standard deviation of the current of all pads is $(2.0\times10^{-8}\pm1.0\times10^{-8})$ A. For this measurement method cells with a current higher than 100 nA count as defect cells. The median current is smaller by a factor

of 16. An advantage of this method is that the current of the defective cells does not influence the neighbouring cells. In the plot, a few defective cells with premature breakdown can be found. The reason why there are so many defective cells is still under investigation and needs to be addressed for future prototype sensors from the same vendor. Another effect only visible with this method is the radial behaviour of the current distribution. In the centre of the sensor, the current is smaller by almost a factor 2 compared to the outside. This is related to lithography problems during production that lead to a radial distribution with no metal overhang on the outer part of the sensor. Finally, it should be mentioned that different currents in the quadrants, as suggested by simulations in Section 3, cannot be observed. The first reason for that is because at -100 V, except for the defective cells, the cells do not break down, and hence no difference due to different breakdown voltages that can be attributed to the design can be observed. Secondly, the current increase due to the lateral spread of the depletion zone cannot occur in this measurement configuration as well. Changing the pad distance for the different quadrants is implemented by changing the cell size. For cells with an area of 1.0 cm^2, increasing or decreasing the cell radius by only 20 µm changes the current only marginally.

5 Summary

The new High Granularity Calorimeter of the CMS experiment will need about 27000 silicon sensors on 8-inch wafers for the CMS Phase-2 upgrade. The design of an 8-inch prototype with 235 pads was shown. For the final design the number of pads will change, depending on the thickness of the sensor. The 120 µm thick sensor will feature 432 pads, whereas the 200 µm and 300 µm thick sensor will have 192 pads. These pad numbers originate from the idea of merging 4 neighbouring cells to form a trigger cell. As these cell should not be split up on the edge of the sensor, the total pad number is strictly constrained.
TCAD simulations show that at the inter-pad region the maximum electric field is located beneath the edge of the metal overhang in the bulk. Additionally, the metal overhang should always be larger than 5 µm. For pad distances larger than 40 µm, the metal overhang can be up to 15 µm to optimize the breakdown voltage. The last section compared two different measurement methods. One is the single needle method, which is the fastest and easiest to perform. However, it suffers from increased currents due to the lateral spread of the depletion region. Hence, single bad cells influence the current of all neighbouring cells and deteriorate the measurement. The second method features seven needles. If done manually, it is cumbersome and time consuming, but the same biasing scheme could be accomplished with a probecard to contact all pads at the same time. This would speed up the measurement time. This biasing configuration delivers the current of a single cell and is not influenced by bad neighbour cells. The preferred way to test sensors, either in the laboratory or at the sensor manufacturers, is therefore the second biasing configuration featuring seven needles.

Acknowledgments

The research leading to these results has been co-funded by the European Commission under the Horizon 2020 Research Infrastructures project AIDA-2020, Grant Agreement 654168.

References

[1] B. Schmidt, *The High-Luminosity upgrade of the LHC: Physics and Technology Challenges for the Accelerator and the Experiments*, *Journal of Physics* **706** (2016) 022002.

[2] CMS collaboration, *The CMS Experiment at the CERN LHC*, *JINST* **3** (2008) S08004.

[3] A.A. Maier, *Sensors for the CMS High Granularity Calorimeter*, *JINST* **12** (2017) C06030.

[4] T. Bergauer et al., *First thin AC-coupled silicon trip sensors on 8-inch wafers*, *NIMA* **830** (2016) 473-479.

[5] CMS collaboration, *Technical Proposal for the Phase-II Upgrade of the CMS Detector*, *CERN-LHCC-2015-010* (2015).

[6] CMS collaboration, *P-Type Silicon Strip Sensors for the new CMS Tracker at HL-LHC*, *JINST* **12** (2017) P06018.

[7] E. Currás et al., *Radiation hardness study of Silicon Detectors for the CMS High Granularity Calorimeter (HGCAL)*, *JINST* **12** (2017) C02056.

[8] Synopsys TCAD, URL:http://www.synopsys.com/.